

Predicting tidal heights for extreme environments: From 25 hr observations to accurate predictions at Jang Bogo Antarctic Research Station, Ross Sea, Antarctica

Do-Seong Byun¹, Deirdre E. Hart²

¹Ocean Research Division, Korea Hydrographic and Oceanographic Agency, Busan 49111, Republic of Korea

²School of Earth and Environment, University of Canterbury, Christchurch 8140, Aotearoa New Zealand

Correspondence to: Deirdre E. Hart (deirdre.hart@canterbury.ac.nz)

Abstract. Accurate tidal height data for the seas around Antarctica are much needed, given the crucial role of these tides in the regional and global ocean, marine cryosphere, and climate processes. However obtaining long term sea level records for traditional tidal predictions is extremely difficult around ice affected coasts. This study evaluates the ability of a relatively new, tidal species based approach, the Complete Tidal Species Modulation with Tidal Constant Corrections (CTSM+TCC) method, to accurately predict tides for a temporary observation station in the Ross Sea, Antarctica, using a record from a neighbouring reference station characterised by a similar tidal regime. Predictions for the ‘mixed, mainly diurnal’ regime of Jang Bogo Antarctic Research Station (JBARS) were made and evaluated based on summertime (2017; and 2018 to 2019) short-term (25 hr) observations at this temporary station, along with tidal prediction data derived from year-long observations (2013) from the neighbouring ‘diurnal’ regime of Cape Roberts (ROBT). Results reveal the CTSM+TCC method can produce accurate (to within ~5 cm Root Mean Square Errors) tidal predictions for JBARS when using short-term (25 hr) tidal data from periods with higher than average tidal ranges (i.e. those at high lunar declinations). We demonstrate how to determine optimal short-term data collection periods based on the Moon’s declination and/or the modulated amplitude ratio and phase lag difference between the diurnal and semidiurnal species predicted from CTSM at ROBT (i.e. the reference tidal station). The importance of using long period tides to improve tidal prediction accuracy is also considered and, finally, the unique tidal regimes of the Ross Sea examined in this paper are situated within a wider Antarctic tidal context using FES2014 model data.

Copyright statement (will be included by Copernicus)

1 Introduction

Conventionally, year-long sea level records are used to generate accurate tidal height predictions via harmonic methods (e.g. Codiga, 2011; Foreman, 1977; Pawlowicz et al., 2002). Obtaining long term records for such tidal analyses is extremely difficult for sea ice affected coasts like that surrounding Antarctica. As a compliment to in situ tidal records, recent work has significantly advanced our understanding of tide models for the shallow seas around Antarctica and Greenland via the assimilation of laser altimeter data and use of Differential Interferometric Synthetic Aperture Radar (DInSAR) imagery, amongst other methods (Padman et al., 2008; 2018; King et al., 2011; Wild et al., 2019). However, Byun and Hart (2015) developed a new approach to successfully predict tidal heights based on as little as 25 hr of sea level records when combined with neighbouring reference site records, using their Complete Tidal Species Modulation with Tidal Constant Corrections (CTSM+TCC) method, on the coasts of Korea and New Zealand. Demonstrating the usefulness of this method for generating accurate tidal predictions for new sites on sea ice affected coasts is the motivation for this study. We focus on the Ross Sea, Antarctica, as our case study area.

Long-term, quality sea level records in the Ross Sea are few and far between, and include observations from gauges operated by New Zealand at Cape Roberts (ROBT); by the United States in McMurdo Sound (see reference to data in Padman et al.,

2003); and by Italy at Mario Zucchelli Station (Gandolfi, 1996), all in the eastern Ross Sea. Permanent sea level gauge installations in this extreme environment must accommodate or somehow avoid surface vents freezing over with sea ice, and damage to subsurface instruments from icebergs. There is also the challenge of securing and preventing damage to the cables that join the subsurface instruments to their onshore data loggers and power supplies, across the seasonally dynamic and harsh coastal and subaerial environments of Antarctic shorelines. At ROBT, these issues have been avoided by sheltering the sea level sensor towards the bottom of a 10 m long hole, drilled through a large shoreline boulder, from its surface ~2 m above the sea and sea ice level, to ~6 m below sea level, below the base of the sea ice (Glen Rowe, Technical Leader Sea Level Data, New Zealand Hydrographic Authority, *pers. comm.* 13 Dec. 2019). In the absence of a suitable permanent gauge site, hydrographic surveys have been conducted at the Korean Jang Bogo Antarctic Research Station (JBARS). Such surveys are best conducted during the summertime predominantly sea ice free window around mid-January to mid-February. Even then, mobile ice (Fig. 1) and severe weather events frequently hinder surveys via instrument damage or loss, not to mention the logistical difficulties of instrument deployment and recovery (Rignot et al. 2000). Accurate tidal records from the Ross Sea and other areas around Antarctica are thus scarce compared to those available from other regions, although these data are much needed given the crucial role of tidal processes around this continent (Han et al., 2005; Jourdain et al., 2018; Padman et al., 2003; 2018).

Floating ice shelves occupy around 75% of Antarctica's perimeter (Padman et al., 2018). Tidal oscillations at the ice-ocean interface influence the location and extent of grounding zones (Padman et al., 2002), and control heat transfer and ocean mixing in cavities beneath the marine cryosphere (Padman et al., 2018) and the calving and drift of icebergs (Rignot et al. 2000). Tides also affect variability in polynyas; seasonal sea ice patterns; and thus the functioning of marine ecosystems. And tides affect the dynamics of landfast sea ice, which provides aircraft landing zones (Han and Lee, 2018).

Accurate Antarctic region tide data are needed for models examining changes in global climate and ocean circulation (Han and Lee, 2018) while coastal tide data are needed for ice mass balance and motion studies (Padman et al., 2008; Rignot et al. 2000; Rosier and Gudmundsson, 2018). Ice thickness is typically measured by subtracting tidal heights from highly accurate but relatively low resolution (temporally or spatially) satellite or in situ observations of ice surface elevation (Padman et al., 2008). Where ice shelves and glacier tongues occur, grounding zone and ice flexure mechanics make ice thickness and motion determination challenging, so that accurate tidal height inputs are crucial (Wild et al. 2019).

In this study, we tested the applicability of Byun and Hart's (2015) CTSM+TCC method in an extreme observation environment using 25 hr short-term records from JBARS, our temporary tidal observation station, and year-long data from ROBT, the neighbouring reference station. Sect. 2 of this paper details the JBARS and ROBT observation data sets used to generate harmonic tidal analysis results and CTSM+TCC tidal predictions. Sect. 3 explains how the CTSM+TCC method was applied and adapted in this case study (with Appendix 1 detailing the calculations), while Sect. 4 demonstrates the CTSM+TCC tidal prediction capability. Sect. 5 discusses the generation of fortnightly tide effects and double tidal peaks; and situates the Ross Sea tides examined in this paper within the wider context of Antarctic tidal regimes.

2 Antarctica's major tides: Observations and background

2.1 Study sites and data records

The Korea Hydrographic and Oceanographic Agency (KHOA) survey team went to JBARS in Northern Victoria Land's Terra Nova Bay, Ross Sea, Antarctica, in the austral summertime of 2017 (Fig. 2) for a preliminary fieldtrip to conduct hydrographic surveys and produce a nautical chart. This mission collected the first, 19 day sea level related record for JBARS: 10 min interval subsurface pressure observations were recorded between 28 Jan. and 16 Feb. 2017 using a bottom-mounted pressure sensor (WTG-256S AAT, Korea) with the data converted to sea level heights using the hydrostatic equation. High-frequency sea level oscillations (<3 hr) were removed from the observation record using a fifth-order low-pass Butterworth filter. Note

that the first and last days of this campaign comprised partial day records, so we excluded these end days from our tidal prediction experiments, since our method requires continuous 25 hr input data (i.e. covering one tidal cycle minimum and, for convenience, starting at midnight). That left 17 days and 1 hour of useable tidal observation data as the basis of the primary JBARS observation record. Note that short-term records >25 hr may be used in CTSM+TCC but, as demonstrated in Byun and Hart (2015), large tidal range (range being twice amplitude) and high data quality have a much greater positive impact on prediction results than any increase in the length of the short-term observation records employed. For the purposes of a full-scale survey, three additional, discontinuous sea level observation records were measured by KHOA at JBARS between 29 Dec. 2018 and 11 Mar. 2019, all at 10 min intervals using the same instrument. Of these, the 20.54 day record produced between 29 Dec. 2018 and 18 Jan. 2019 comprised relatively high quality data with small residuals (i.e. observations minus predictions). We used this additional dataset (hereafter referred to as the JBARS 2019 observations) to verify CTSM+TCC method tidal predictions generated from input parameters derived from ‘daily’ (25 hr) slices of the 2017 sea level records. Due to the short duration of the KHOA survey team’s forays into the Ross Sea, and in the absence of a permanent tide station at JBARS, it was not possible to collect the year-long sea level records that are commonly employed to obtain reliable tidal harmonic constants for tidal prediction. Approximately 269 km south of JBARS, there is a permanent tidal observation station named after its location on Cape Roberts (ROBT), operated by Land Information New Zealand (LINZ) and recording at intervals since November 1990 (Fig. 2). Five minute interval seawater pressure data have been collected at ROBT since November 2011 using GEOKON 4500 series Standard Piezometers, vented to the atmosphere, with this data converted to sea level heights using the hydrostatic equation. Part of the 2017 record from this site was unavailable online at the time of starting this research, so instead we chose as our reference records the 2013 ROBT sea level data, a quality year-long dataset with few missing points.

2.2 Tidal characteristic analyses and descriptions

Using the T_TIDE toolbox (Pawlowicz et al., 2002), we obtained the tidal harmonic constants of the 8 and 6 major tidal constituents for ROBT and JBARS, respectively (Table 1). Also the inference method was used to infer the P_1 constituent from the K_1 , and the K_2 constituent from the S_2 , with their amplitude ratios and phase lag differences obtained from harmonic analysis of the long-term ROBT reference station records. Analyses revealed that the two main diurnal (O_1 and K_1) and semidiurnal (M_2 and S_2) tides had similar amplitudes at the two stations, with the diurnal (semidiurnal) amplitudes being slightly larger (smaller) at ROBT than at JBARS, and the phase lags of all four tides having only slightly different values at the two stations. The amplitude differences result in slightly different tidal form factors at the two sites (e.g., F in Table 1).

3 Using the CTSM+TCC tidal prediction methodology in the Ross Sea

Having analysed the tidal harmonic constants at the two stations, we then employed the CTSM+TCC method (Byun and Hart, 2015) to generate tidal height predictions for JBARS, our ‘temporary’ tidal observation station (subscript o), using ROBT as the ‘reference’ station (subscript r). This prediction approach (see Appendix 1 for the detailed calculations, and Byun and Hart (2015) for explanation of procedure development) is based on:

- (i) using long-term (1 year, in our case) reference station records (LH_r) and CTSM calculations to make an initial anytime (τ) tidal prediction ($\eta_r(\tau)$), which involves summing tidal species’ heights for the reference station (Fig.3);
- (ii) comparing the tidal harmonic constants (amplitude ratios and phase lag differences) of representative tidal constituents (e.g., M_2 and K_1) for each tidal species between the temporary and reference stations (Fig. 4), calculated using T_TIDE and concurrent short-term records (≥ 25 hr duration, starting at midnight) from the temporary (SH_o) and reference (SH_r) stations; and

(iii) using the step (ii) comparative data and the TCC calculations for each tidal species to adjust the $\eta_r(\tau)$ tidal species' heights in order to generate accurate, anytime tidal height predictions for the temporary tidal station ($\eta_o(\tau)$).

In this Ross Sea case study we used the 2017 JBARS tidal observation records (i.e. 17.04 days from 00:00 29 Jan. to 01:00 15 Feb.) as a source of SH_o , keeping the second JBARS 2019 observation record for evaluation purposes.

Importantly, this method assumes that the reference and temporary tidal stations are situated in neighbouring regimes with similar dominant tidal constituent and tidal species characteristics, and that the tidal properties between the two stations remain similar through time. As explained above, both JBARS and ROBT have tidal regimes that are primarily dominated by diurnal tides. LH_r can come from any time period, but must comprise high quality (e.g. few missing data) tidal height observations throughout.

Byun and Hart (2015) recommended the use of short-term records gathered during periods of calm weather, to minimise errors due to atmospheric influences. They employed observational data for both SH_o and SH_r but as demonstrated in this paper the method can also be applied using tidal predictions as a source of SH_r . This adjustment in approach arose since for the 2017 JBARS observation time period, the concurrent 2017 ROBT records available online (LINZ, 2019) had multiple missing data. We solved this issue by producing a year-long synthetic 2017 record for ROBT using T_TIDE (Pawlowicz et al., 2002) and the 2013 (i.e. LH_r) observational record as input data. The 17.04 days of predicted tides that were concurrent with the 2017 JBARS observation record were then used as our SH_r source. While this CTSM+TCC method adjustment was procedurally small, it represents an important adaptation in the context of generating tidal predictions for stations situated in extreme environments, since concurrent temporary and reference station observations might be rare in such contexts.

When using CTSM+TCC, if the available temporary tidal station observation record covers multiple days, it is best practice to experiment by generating multiple $\eta_o(\tau)$, each using different concurrent pairs of SH_o and SH_r daily data slices in step (ii) above, to produce daily amplitude ratios and phase lag differences between the two stations for the diurnal K_1 and semidiurnal M_2 tidal constituents. Comparisons are then made between the different $\eta_o(\tau)$ data sets produced and the original temporary station observations, to determine the optimal 25 hr window to use: once selected, tidal height predictions can be generated for the temporary observation station for any time period. Thus, 17 individual 25 hr duration data slices were clipped from the 2017 JBARS observation records and from the concurrent ROBT predictions, forming 17 pairs of SH_o and SH_r 'daily' slices. Each paired data set was then used with LH_r to generate tidal height predictions for JBARS covering both the 2017 and 2019 KHOA observation campaign time periods. Comparisons were made between the complete JBARS observations and the 17 prediction data sets generated for each campaign to identify which 25 hr short-term data window produced optimal $\eta_o(\tau)$ results.

147 4 Results

148 4.1 Tidal prediction evaluation

CTSM+TCC was used to produce 17 different JBARS tidal prediction data sets for the period 29 Jan. to 14 Feb. 2017, based on harmonic analysis results of the 'daily' (25 hr) K_1 and M_2 amplitudes and phase lags at our two tidal observation stations. Figure 5a illustrates one such tidal height prediction data set, in comparison to the observed tides. In order to evaluate the 17 different prediction results, each prediction data set was compared with the concurrent JBARS field observations via Root Mean Square Error (RMSE) and coefficient of determination (R^2) statistics.

RMSEs between the 2017 observations and predictions ranged from 4.26 cm to 20.56 cm, while R^2 varied from 0 to 0.94, across the 17 'daily' experiments (Fig. 6). Eleven of the experiments produced accurate results (i.e. excluding those derived from 31 Jan.; and 1 to 4 and 14 Feb. data slices). Daily datasets from periods with relatively high tidal ranges (>83.5 cm) produced predictions with RMSEs <5 cm and R^2 values >0.92 . The maximum tidal range occurred on 9 Feb., with step (ii) data slices from this date producing predictions with a low (but not the lowest) RMSE (4.81 cm). The predictions with the

lowest RMSE (4.259 cm) and highest R^2 value (0.941) were produced using data slices from one day earlier, 8 Feb. 2017 (Fig. 5a and Fig. 6). In contrast to the successful prediction datasets, that based on using the 2 Feb. 2017 data slices in step (ii) of the method produced predictions with very high RMSE (20.56 cm) and very low R^2 (0.00) values (Fig. 6). The 2 Feb. 2017 tides were characterised by the smallest tidal range (11.95 cm) of the JBARS record, during a period of low lunar declination. Interestingly, RMSEs and R^2 values between the 2019 CTSM+TCC tidal predictions and observations were almost identical to those of the 2017 comparisons, revealing that our approach performed consistently across different prediction years. As in the 2017 experiments, the 2019 prediction dataset made using the 8 Feb. 2017 data slices (i.e., in step (ii) of the method) produced the lowest RMSE (5.3 cm) and highest R^2 (0.913) values of the 2019 experiments (Fig. 5b). Across both the 2017 and 2019 prediction time periods, the RMSE and R^2 results varied in relation to the JBARS tidal range, with greater accuracy evident in predictions made using step (ii) 2017 data slices from periods with above average tidal ranges. In the JBARS area of the Ross Sea during the 2017 short-term observation period, above average tidal ranges corresponded to the period when the moon was near its greatest northern declination (Fig. 6). Collectively these results show that the CTSM+TCC method can be used successfully to predict tidal heights for JBARS, when using short-term observation records gathered from periods at high lunar declination, and thus above average tidal ranges, with relatively calm weather, together with observation or prediction records from the neighbouring reference station ROBT.

4.2 Determining the ideal short-term sea level observation period when using CTSM+TCC

The previous section verified that the CTSM+TCC method can be used to generate accurate tidal predictions based on 25 hr sea level records, from periods with above average tidal ranges, for a temporary station in a mixed, mainly diurnal regime and a reference station in a diurnal regime. The question arises as to how to determine optimal observation days in such settings to produce the most accurate tidal predictions.

For semidiurnal or mixed, mainly semidiurnal tidal regimes, we can estimate preferred temporary station observation days, those with the largest tidal ranges, based on the moon's phase, without reference to tide tables. That is, spring tides commonly occur just a day or two after the full and new moon, which reoccurs at a period of 14.76 days. The time lag between the full or new moon and the spring tide is called the age of the tide (AT).

Similarly, in a diurnal tide regime or a mixed, mainly diurnal tide regime, preferred temporary station observation days can be estimated based on the lunar declination (Fig. 7), which varies at a period of 13.66 days. That is, maximum tidal range days can be estimated for JBARS based on the day of the Moon's greatest northern (GN) and southern (GS) declinations. The time between the Moon's semi-monthly GN and GS declinations and their effects on tidal range, called the age of diurnal inequality (ADI), is commonly 1 to 2 days. The GN and GS lunar declinations during our temporary station summertime observation periods occurred on 8 Feb. 2017 (GN) and on 6 Jan. 2019 (GS) respectively (Fig. 7), with the maximum diurnal tides at JBARS expected around 1 day after each lunar declination peak.

Thus, when planning to use the CTSM+TCC tidal prediction method for places characterised by diurnal or mixed, predominantly diurnal tidal regimes, we can use knowledge of the moon's declination to select potential sea level observation days.

4.3 Comparison of ROBT and JBARS tidal species characteristics

The CTSM+TCC tidal prediction method is based on the assumption that the tidal harmonic characteristics of each tidal species are very similar between the temporary and reference stations. This is because the reference station tidal species' CTSMs form the basis of the tidal predictions for the temporary observation station. To test the validity of this assumption, we examined the phase lag (G) differences of the two major diurnal and semidiurnal tidal constituents using ADI and AT , calculated as:

$$ADI \text{ (day)} = \left(\frac{G_{K_1} - G_{O_1}}{\omega_{K_1} - \omega_{O_1}} \right) / 24, \text{ and} \quad (1)$$

$$AT \text{ (day)} = \left(\frac{G_{S_2} - G_{M_2}}{\omega_{S_2} - \omega_{M_2}} \right) / 24, \quad (2)$$

where ω_{K_1} ($= 15.0410686^\circ \text{ hr}^{-1}$), ω_{O_1} ($= 13.9430356^\circ \text{ hr}^{-1}$), ω_{S_2} ($= 30.0000000^\circ \text{ hr}^{-1}$), and ω_{M_2} ($= 28.9841042^\circ \text{ hr}^{-1}$) are the angular speeds of the K_1 , O_1 , S_2 and M_2 tides, respectively. Results revealed that the *ADI* are very similar, and there is <1 day *AT* difference, between ROBT and JBARs respectively (Table 1), indicating that the tidal characteristics of the representative tidal constituents for each species between the two stations are very similar, in particular the dominant diurnal species. Note that the negative *AT* values in Table 1 are an unusual feature of the Ross Sea tides, given that elsewhere spring tides commonly occur a day or two after the full and new moon. The *ADI* and *AT* similarities between our two stations explain why we found the CTSM+TCC method successful in generating the Ross Sea tidal predictions.

5 Discussion

5.1 Explaining fortnightly tide effects and double tide peaks in the Ross Sea tidal predictions

We have demonstrated that the CTSM+TCC approach can produce reasonably accurate tidal predictions (RMSE <5 cm, $R^2 > 0.92$) for a new site in the Ross Sea, Antarctica, based on 25 hr temporary station observation records from periods with above average tidal ranges, plus neighbouring reference station records. Our results compare favourably with those of Han et al. (2013), who reviewed the tidal height prediction accuracy of 4 models for Terra Nova Bay, Ross Sea: these models generated similar quality results to our CTSM+TCC results, with R^2 values between 0.876 and 0.907, and RMSEs ranging from 3.6 to 4.1 cm. However, as shown in Fig. 5, our results contain a changing fortnightly timescale bias in estimates. This error pattern likely resulted from our application of CTSM+TCC considering only 2 major tidal species (diurnal and semidiurnal) whilst ignoring several long period and small amplitude short period tides.

Table 2 summarises the characteristics of 6 long-period tides (S_a , S_{sa} , MS_m , M_m , M_f , MS_f) at the ROBT station, derived from tidal harmonic analysis of year-long (2013) in situ observation records. Note that since the ROBT observation record was derived from seawater pressure measurement, and thus includes proportionately large non-tidal (atmospheric) sea level variations, caution should be exercised in comparing the harmonic analysis results of the non-astronomical constituents, which are affected by seawater density and atmospheric forcing (i.e. S_a and S_{sa}).

To investigate the main cause of the apparent fortnightly prediction biases in our results, we examined the effects of two fortnightly tidal constituents (M_f , and MS_f) at ROBT using T_TIDE. Three 2019 tidal prediction experiments were conducted:

- *Srun* excluded all long-period tides (see list of exclusions in Table 2);
- *Run1* was based on *Srun* but also incorporated M_f ; and
- *Run2* was based on *Srun* but also incorporated M_f and MS_f ;

with T_TIDE predictions made for each case. Comparisons between *Run1* and *Srun* predictions revealed that exclusion of the M_f tide (2.7 cm amplitude) can produce prediction biases during periods of lunar declination change, with comparisons between *Run2* and *Run1* results revealing that the additional exclusion of the MS_f tide (1.2 cm amplitude) intensifies the biases. While these results elucidate an issue with predicting Ross Sea tides based on the diurnal and semidiurnal species alone, the aforementioned differences in gauge and record types in themselves can also result in different harmonic analysis results and, in turn, different prediction results.

Rosier and Gudmundsson (2018) found that ice flows are modulated at various tidal frequencies, including that of the MS_f tide. However, because these tides' amplitudes have small signal-to-noise ratios (<1) with large standard errors (Table 2), caution should be exercised when elucidating fortnightly tide effects using these constituents. Nevertheless, studies indicate that incorporating major and minor tidal constituents, including long period tides, into tidal predictions may be advantageous for their use in ice flow and ice-ocean front modelling specifically (e.g. Rignot et al., 2000; Rosier and Gudmundsson, 2018).

238 Consideration of additional, long period tides in predictions is one recommendation we have for future work on improving
 239 tidal predictions for Ross Sea coasts.

240 Another characteristic of our results needing explanation is the double tidal peaks evident in both the tidal observations and
 241 predictions at JBARS. These peaks occur, for example, in Fig. 5b between Jan. 11th and 17th, 2019. To explore why these
 242 double peaks occur, we generated JBARS tidal height predictions using Eq. (A1) and the 2019 tidal constants listed in Table
 243 1 for the two major diurnal and semidiurnal tides. Fig. 8a shows separately the resulting diurnal (with their period of 13.66
 244 days) and semidiurnal (with their period of 14.77 days) species' tide predictions. The combination of these out-of-phase tidal
 245 species generates double peaks (or double troughs) around low and high tide (Fig. 8b) for periods when the diurnal tide
 246 amplitude is low, due to the similar amplitude K_1 and O_1 tides cancelling each other out across a fortnight, allowing the
 247 combined M_2 and S_2 amplitude to temporarily approach or exceed that of the combined K_1 and O_1 tides (Fig. 8c). Since the
 248 semidiurnal tides are slightly stronger, and the diurnal tides are slightly weaker, at JBARS compared to at ROBT (Table 1),
 249 these double tide peaks occur more commonly at JBARS.

250 5.2 Understanding the contrasting tidal environments around Antarctica

251 Figure 9 illustrates the form factors of tidal regimes in the seas surrounding Antarctica, according to FES2014 model data.
 252 There are large areas characterised by diurnal ($F > 3$); mixed, mainly diurnal ($1.5 < F < 3$); and mixed, mainly semidiurnal
 253 ($0.25 < F < 1.5$) forms. Only in a small area half-way along the Weddell Sea coast of the Antarctic Peninsula (at 72°S) do tides
 254 exhibit a semidiurnal form ($F < 0.25$). The Weddell Sea is dominated by mixed, mainly semidiurnal tides, excepting the
 255 semidiurnal area mentioned and another small area exhibiting diurnal tides ($F > 3$) at around 76.5°S, where amphidromic points
 256 (i.e. zero amplitudes) occur for both the M_2 and S_2 tides. Strong diurnal tides predominate in the Ross Sea area of West
 257 Antarctica, around to the Amundsen Sea. In addition, a small area near Prydz Bay (Fig. 2) in East Antarctica exhibits diurnal
 258 and mixed mainly diurnal tides. The rest of the seas surrounding Antarctica are predominantly characterised by mixed, mainly
 259 semidiurnal tides.

260 Since diurnal tides have larger nodal amplitude factor and nodal angle variations than semidiurnal tides (Pugh and Woodworth,
 261 2014), areas like the Ross Sea will have larger variations in tidal height across the 18.61 year lunar nodal cycle compared to
 262 areas like the Weddell Sea. As the nodal amplitude factor variations of the diurnal and semidiurnal tides are out of phase, this
 263 leads to differing tidal responses around Antarctica over 18.61 years, particularly between the Ross and Weddell Seas (see
 264 details for ROBT in Byun and Hart, 2019). Given that CTSM+TCC is based on modulated tidal amplitude and phase lag
 265 corrections for each diurnal and semidiurnal species, this approach is applicable in studying a continent with such a diversity
 266 of tidal regime types.

267 6 Conclusions

268 This paper has demonstrated the usefulness of the CTSM+TCC method for tidal prediction in extreme environments, where
 269 long-term tidal station installations are difficult, using the Ross Sea in Antarctica for our case study. Here CTSM+TCC
 270 methods can be employed for accurate tidal height predictions for a temporary tidal observation station using short-term (≥ 25
 271 hr) sea level records from this site, plus long-term (1 year) tidal records from a neighbouring reference tidal station. Essentially
 272 the temporary and reference station sites must share similarities in their main tidal constituent and tidal species characteristics
 273 for CTSM+TCC to produce acceptable results.

274 Using this approach, an initial tidal prediction time series is generated for the temporary station using CTSM and the reference
 275 station long-term records. The temporary station predicted time series can then be adjusted via TCC of each tidal species,
 276 based on harmonic comparisons between the short-term temporary station observation record and its corresponding modelled

277 predictions, leading to improved accuracy in the tidal predictions. The modulated amplitude ratio and phase lag difference
278 between diurnal and semidiurnal species predicted from CTSM at the reference station can be used as an indicator for selecting
279 optimal short term observation dates at a temporary tidal station.
280 This paper has further demonstrated that the CTSM+TCC approach can be employed successfully in the absence of concurrent
281 short-term (25 hr) records from the reference station, since a tidal harmonic prediction program can be used to produce a
282 synthetic short-term record for the reference station, based on a quality long-term (1 year) record from that site.
283 The proper consideration of long-period tides in the CTSM+TCC approach remains a challenge, as outlined in this study, with
284 the solutions to this issue likely to improve tidal predictions further. However, this study demonstrates that the CTSM+TCC
285 method can already produce tidal predictions of sufficient accuracy to aid local polar station maritime operations, as well as
286 starting to help resolve gaps in the spatial coverage of tidal height predictions for scientists studying important issues, such as
287 the rate and role of ice loss along polar coastlines.

288 **Code Availability**

289 The T_TIDE based CTSM code is available from https://au.mathworks.com/matlabcentral/fileexchange/73764-ctsm_t_tide.

290 **Data Availability**

291 The sea level data used in this paper are available from LINZ (2019) for selected ROBT records, with the remaining ROBT
292 records available by email application (customersupport@linz.govt.nz); and the JBARS records used are available on request
293 from KHOA (infokhoa@korea.kr). Details of the FES2014 tide model are found in Carrère et al. (2016) and via
294 <https://www.aviso.altimetry.fr/en/data/products/auxiliary-products/global-tide-fes.html>.

295

297 This appendix describes the calculations involved in using the CTSM+TCC approach as employed in this Ross Sea, Antarctica,
 298 case study. For a fuller description of the development of this approach and its application in semidiurnal and mixed, mainly
 299 semidiurnal tidal regime settings, see Byun and Hart (2015).

300 As explained in the main body of this paper, we used 25 hr slices of the 2017 short-term observations from JBARS (SH_o), our
 301 temporary tidal observation station (subscript *o*), and 2013 year-long observations (LH_r) and 2017 short-term tidal predictions
 302 (SH_r, concurrent with SH_o) from ROBT, our reference tidal station (subscript *r*), as the basis of JBARS tidal prediction
 303 calculations. We then employed the full 17.04 day 2017 JBARS tidal observation data set, and an additional 21.54 day 2019
 304 JBARS tidal observation dataset, to evaluate the success of the CTSM+TCC tidal prediction calculations for this site.

305 The CTSM+TCC, expressed as the summation of each tidal species cosine function, includes three key steps:

- 306 (i) calculating each tidal species' modulation at the reference tidal station;
- 307 (ii) comparing the tidal harmonic constants between the temporary observation and reference stations (e.g., the tidal
 308 amplitude ratios and phase lag differences of each representative tidal constituent for each tidal species calculated
 309 from concurrent observation records between two stations); and
- 310 (iii) adjusting the tidal species modulations calculated in the first step using the correction factors calculated in the
 311 second step to produce predictions for the temporary tidal station.

312 As a first step, tidal height predictions for the temporary station ($\eta_o(\tau)$) were initially derived from reference station predictions
 313 ($\eta_r(\tau)$) on the assumption that the tidal properties between the two stations remain similar through time. Using the modulated
 314 amplitude ($A_r^{(s)}$) and the modulated phase lag ($\varphi_r^{(s)}$) for each tidal species, this step is expressed as:

$$315 \quad \eta_r(\tau) = \sum_{s=1}^k A_r^{(s)}(\tau) \cos(\omega_R^{(s)}t - \varphi_r^{(s)}(\tau)) \quad (A1)$$

316 with

$$317 \quad A_r^{(s)}(\tau) = \sqrt{\sum_{i=1}^m [f_i^{(s)}(\tau) a_i^{(s)}]^2 + 2 \sum_{i=1}^{m-2} \sum_{j=i+1}^m [f_i^{(s)}(\tau) a_i^{(s)}][f_j^{(s)}(\tau) a_j^{(s)}] \cos\{(\omega_i^{(s)} - \omega_j^{(s)})t + [V_i^{(s)}(t_0) + u_i^{(s)}(\tau) - G_i^{(s)}] - [V_j^{(s)}(t_0) + u_j^{(s)}(\tau) - G_j^{(s)}]\}}$$

318 (A2)

319 and

$$320 \quad \varphi_r^{(s)}(\tau) = \tan^{-1} \left(\frac{\sum_{i=1}^m f_i^{(s)}(\tau) a_i^{(s)} \sin[(\omega_i^{(s)} - \omega_R^{(s)})t + V_i^{(s)}(t_0) + u_i^{(s)}(\tau) - G_i^{(s)}]}{\sum_{i=1}^m f_i^{(s)}(\tau) a_i^{(s)} \cos[(\omega_i^{(s)} - \omega_R^{(s)})t + V_i^{(s)}(t_0) + u_i^{(s)}(\tau) - G_i^{(s)}]} \right) \quad (A3)$$

321 where superscript *s* denotes the type of tidal species (e.g., 1 for diurnal species and 2 for semidiurnal species); *m* is the number
 322 of tidal constituents; *t*₀ is the reference time; *t* is the time elapsed since *t*₀; and $\tau = t_0 + t$; $\omega_i^{(s)}$ are the angular frequencies
 323 of each tidal constituent (subscripts *i* and *j*); $\omega_R^{(s)}$ are the angular frequencies of each tidal constituent representing a tidal
 324 species (subscript *R*); with the dominant tidal constituent of each tidal species used as the representative for that species (e.g.,
 325 K₁ and M₂ are used as representative of the diurnal and semidiurnal species, respectively). For each tidal constituent, $a_i^{(s)}$ and
 326 $G_i^{(s)}$ are the tidal harmonic amplitudes and phase lags (referenced to Greenwich); $f_i^{(s)}(\tau)$ is the nodal amplitude factor of each
 327 tidal constituent; $u_i^{(s)}(\tau)$ is the nodal angle; and $V_i^{(s)}(t_0)$ is the astronomical argument. T_TIDE was used for tidal harmonic
 328 analysis as well as for calculation of the nodal amplitude factors; nodal angles; and astronomical arguments; for the
 329 representative tidal constituents.

330 As the second step, under the 'credo of smoothness' assumption that the admittance or 'ratio of output to input' does not
 331 change significantly between constituents of the same species (Munk and Cartwright, 1966; Pugh and Woodworth, 2014), the
 332 amplitude ratio and phase lag difference of each representative tidal constituent for each tidal species between the temporary
 333 and reference stations were calculated from the results of tidal harmonic analyses of concurrent 25 hr data slices (starting at

334 00.00) from the temporary observation and reference tidal stations (i.e. from SH_o and SH_r). The process of selecting the optimal
 335 25 hr window for the concurrent data slices from amongst the 17.04 days of available records is explained in Sect. 3.
 336 Once this 2017 window was selected, the third step involved adjusting the tidal predictions at the reference station calculated
 337 from Eq. (A1), to represent those for the temporary station ($\eta_o(\tau)$), by substituting the daily (i.e. SH_o and SH_r) amplitude ratios
 338 $\left(\frac{a_o^{(s)}}{a_r^{(s)}}\right)$ and phase lag differences $(G_o^{(s)} - G_r^{(s)})$ for the tidal constituents (K_1 and M_2) representing the diurnal and semidiurnal
 339 tidal species between the temporary and reference stations into Eq. (A1) as follows (Byun and Hart, 2015):

$$340 \quad \eta_o(\tau) = \sum_{s=1}^k A_o^{(s)}(\tau) \cos\left(\omega_R^{(s)} t - \varphi_o^{(s)}(\tau)\right) \quad (A4)$$

$$341 \quad \text{with } A_o^{(s)}(\tau) = A_r^{(s)}(\tau) \left(\frac{a_o^{(s)}}{a_r^{(s)}}\right), \text{ and} \quad (A5)$$

$$342 \quad \varphi_o^{(s)}(\tau) = \varphi_r^{(s)}(\tau) + G_o^{(s)} - G_r^{(s)} \quad (A6)$$

343 Substituting Eqs. (A5) and (A6) into Eq. (A4), $\eta_o(\tau)$ can be expressed as:

$$344 \quad \eta_o(\tau) = \sum_{s=1}^k A_r^{(s)}(\tau) \left(\frac{a_o^{(s)}}{a_r^{(s)}}\right) \cos\left[\omega_R^{(s)} t - (\varphi_r^{(s)}(\tau) + G_o^{(s)} - G_r^{(s)})\right] \quad (A7)$$

345

346 The T_TIDE based CTSM code is available from https://au.mathworks.com/matlabcentral/fileexchange/73764-ctsm_t_tide.

347 **Author contribution**

348 D-SB conceived of the tidal prediction idea behind this paper, and drafted initial results sections. Both authors worked on
349 initial and final versions of the full manuscript.

350 **Competing interests**

351 The authors declare that the research was conducted in the absence of any commercial or financial relationships that could be
352 construed as a potential conflict of interest.

353 **Special issue statement (will be included by Copernicus)**

354 **Acknowledgements**

355 We are grateful to Land Information New Zealand (LINZ), and the Hydrographic Survey Division of the Korea Hydrographic
356 and Oceanographic Agency (KHOA), for supplying the tidal data used in this research. A special thank you to Glen Rowe
357 from LINZ for sharing his extensive knowledge of the Cape Roberts sea level gauge site and its records, and to a KHOA
358 colleague for providing the Fig. 1 photograph. Further, we gratefully thank Ms. Hyowon Kim at KHOA for her kind assistance
359 with drafting figures. We are also grateful to Philip Woodworth, Glen Rowe and an anonymous reviewer for comments that
360 greatly helped us improve our manuscript.

361 **References**

362 Byun, D.-S. and Hart, D. E.: On robust multi-year tidal prediction using T_TIDE, *Ocean Sci. J.*, 54, 685-691,
363 doi.org/10.1007/s12601-019-0028-4, 2019.

364 Byun, D.-S. and Hart, D. E.: Predicting tidal heights for new locations using 25h of in situ sea level observations plus reference
365 site records: A complete tidal species modulation with tidal constant corrections, *J. Atmos. Ocean. Tech.*, 32, 350-371,
366 doi.org/10.1175/JTECH-D-14-00030.1, 2015.

367 Carrère L., Lyard, F., Cancet, M., Guillot, A. and Picot, N.: FES 2014, a new tidal model - validation results and perspectives
368 for improvements, Presentation to ESA Living Planet Conference, Prague, 2016.

369 Codiga, D. L.: Unified Tidal Analysis and Prediction Using the UTide Matlab Functions, Technical report 2011-01, Graduate
370 School of Oceanography, University of Rhode Island, 2011.

371 Foreman, M. G. G.: Manual for Tidal Heights Analysis and Prediction, Pacific Marine Science Report, 77-10, 1977.

372 Gandolfi, S.: Terra Nova Bay Permanent Tide Gauge Observatory Site,
373 https://www.geoscience.scar.org/geodesy/perm_ob/tide/terranova.htm, last access 4 Feb. 2020, 1996.

374 Han, H. and Lee, H.: Glacial and tidal strain of landfast sea ice in Terra Nova Bay, East Antarctica, observed by interferometric
375 SAR techniques, *Remote Sens. Environ.*, 209, 41–51, doi.org/10.1016/j.rse.2018.02.033, 2018.

376 Han, H., Lee, J., and Lee, H.: Accuracy assessment of tide models in Terra Nova Bay, East Antarctica, for glaciological studies
377 of DDInSAR technique, *Korean Journal of Remote Sensing*, 29, 375–387, 2013.

378 Han, S. C., Shum, C. K., and Matsumoto, K.: GRACE observations of M2 and S2 ocean tides underneath the Filchner-Ronne
379 and Larsen ice shelves, Antarctica, *Geophys. Res. Lett.*, 32, L20311, doi.org/10.1029/2005GL024296, 2005.

380 Jourdain, N. C., Molines, J.-M., Le Sommer, J., Mathiot, P., Chanut, J., de Lavergne, C., and Madec, G.: Simulating or
381 prescribing the influence of tides on the Amundsen Sea ice shelves, *Ocean Model.*, 133, 44–55,
382 doi.org/10.1016/j.ocemod.2018.11.001, 2018.

383 King, M. A., Padman, L., Nicholls, K., Clarke, P. J., Gudmundsson, G. A., Kulesa, B., and Shepherd, A.: Ocean
384 tides in the Weddell Sea: New observations on the Filchner-Ronne and Larsen C ice shelves and model validation, *J. Geophys.*
385 *Res.*, 116, C06006, doi.org/10.1029/2011JC006949, 2011.

386 LINZ, Land Information New Zealand: Sea level data downloads, [http://www.linz.govt.nz/sea/tides/sea-level-data/sea-level-](http://www.linz.govt.nz/sea/tides/sea-level-data/sea-level-data-downloads)
387 [data-downloads](http://www.linz.govt.nz/sea/tides/sea-level-data/sea-level-data-downloads), last access 2019.

388 Munk, W. H. and Cartwright, D. E.: Tidal spectroscopy and prediction, *Math. Phys. Sci.*, 259, 533-581,
389 doi.org/10.1098/rsta.1966.0024, 1966.

390 Padman, L., Erofeeva, S., and Fricker, H.: Improving Antarctic tide models by assimilation of ICESat laser altimetry over ice
391 shelves, *Geophys. Res. Lett.*, 35, 122504, doi.org/10.1029/2008GL035592, 2008.

392 Padman, L., Erofeeva, S., and Joughin, I.: Tides of the Ross Sea and Ross Ice Shelf cavity, *Antarct. Sci.*, 15, 31–40,
393 doi.org/10.1017/S0954102003001032, 2003.

394 Padman, L., Fricker, H., Coleman, R., Howard, S., and Erofeeva, L.: A new tide model for the Antarctic ice shelves and seas,
395 *Ann. Glaciol.*, 34, 247–254, doi.org/10.3189/172756402781817752, 2002.

396 Padman, L., Siegfried, M., and Fricker, H.: Ocean Tide Influences on the Antarctic and Greenland Ice Sheets, *Rev. Geophys.*,
397 56, 142–184, doi.org/10.1002/2016RG000546, 2018.

398 Pawlowicz, R., Beardsley, B., and Lentz, S.: Classical tidal harmonic analysis including error estimates in MATLAB using
399 T_TIDE, *Comput. Geosci.*, 28(8), 929-937, doi.org/10.1016/S0098-3004(02)00013-4, 2002.

400 Pugh, D. T.: Tides, Surges and Mean Sea-Level: A Handbook for Engineers and Scientists, Wiley, Chichester, United
401 Kingdom, 1987.

402 Pugh, D. T. and Woodworth, P. L.: Sea-level science: Understanding tides, surges, tsunamis and mean sea-level changes,
403 Cambridge University Press, United Kingdom, doi.org/10.1080/00107514.2015.1005682, 2014.

404 Rignot, E., Padman, L., MacAyeal, D., and Schmeltz, M.: Observation of ocean tides below the Filchner and Ronne Ice
405 Shelves, Antarctica, using synthetic aperture radar interferometry: Comparison with tide model predictions, *J. Geophys. Res.-*
406 *Oceans*, 105, 19615–19630, doi.org/10.1029/1999JC000011, 2000.

407 Rosier, S. H. R. and Gudmundsson, G. H.: Tidal bending of ice shelves as a mechanism for large-scale temporal variations in
408 ice flow, *The Cryosphere*, 12, 1699–1713, doi.org/10.5194/tc-12-1699-2018, 2018.

409 Wild, C. T., Marsh, O. J., and Rack, W.: Differential interferometric synthetic aperture radar for tide modelling in Antarctic
410 ice-shelf grounding zones, *The Cryosphere*, 13(12), 3171-3191, doi.org/10.5194/tc-13-3171-2019, 2019.

411 **Table 1. Major tidal harmonic results for diurnal and semidiurnal constituents from harmonic analyses of sea level observations:**
412 **the year-long (2013) record from Cape Roberts (ROBT), and 17.04 day record (29 Jan. to 15 Feb. 2017) and 20.54 day record (29**
413 **Dec. 2018 to 18 Jan. 2019) from Jang Bogo Antarctic Research Station (JBARS) in the Ross Sea (see source details in Sect. 2). For**
414 **the JBARS tidal harmonic analyses, the inference method was used to infer the P_1 constituent from the K_1 , and the K_2 constituent**
415 **from the S_2 , with their amplitude ratios and phase lag differences obtained from harmonic analysis of the long-term ROBT 2013**
416 **reference station record.**

Tidal constituents & characteristics		ROBT (2013) 369 days		JBARS (2017) 17.04 days		JBARS (2019) 20.54 days	
		Amp. (cm)	Pha. (°)	Amp. (cm)	Pha. (°)	Amp. (cm)	Pha. (°)
Diurnal	O_1	21.1	202	19.6	208	16.0	208
	K_1	20.5	217	16.3	214	14.9	216
	P_1	6.6	215	5.2	213	4.8	214
	Q_1	4.4	190	-	-	-	-
Semidiurnal	M_2	5.3	5	6.7	4	6.3	34
	S_2	4.9	309	6.4	329	5.7	320
	N_2	3.8	255	-	-	-	-
	K_2	1.8	315	2.4	333	2.4	328
F		4.1 (diurnal form)		2.7 (mixed, mainly diurnal)		2.6 (mixed, mainly diurnal)	
ADI (day)		0.57		0.23		0.30	
AT (day)		-2.30		-1.44		-2.87	

417 **Note: Amp. denotes amplitude; Pha. denotes phase lag, referenced to 0° Greenwich; F is the amplitude ratio of the ($K_1 + O_1$)/($M_2 +$**
418 **S_2) tides; and ADI and AT denote the age of diurnal inequality and the age of the tide.**

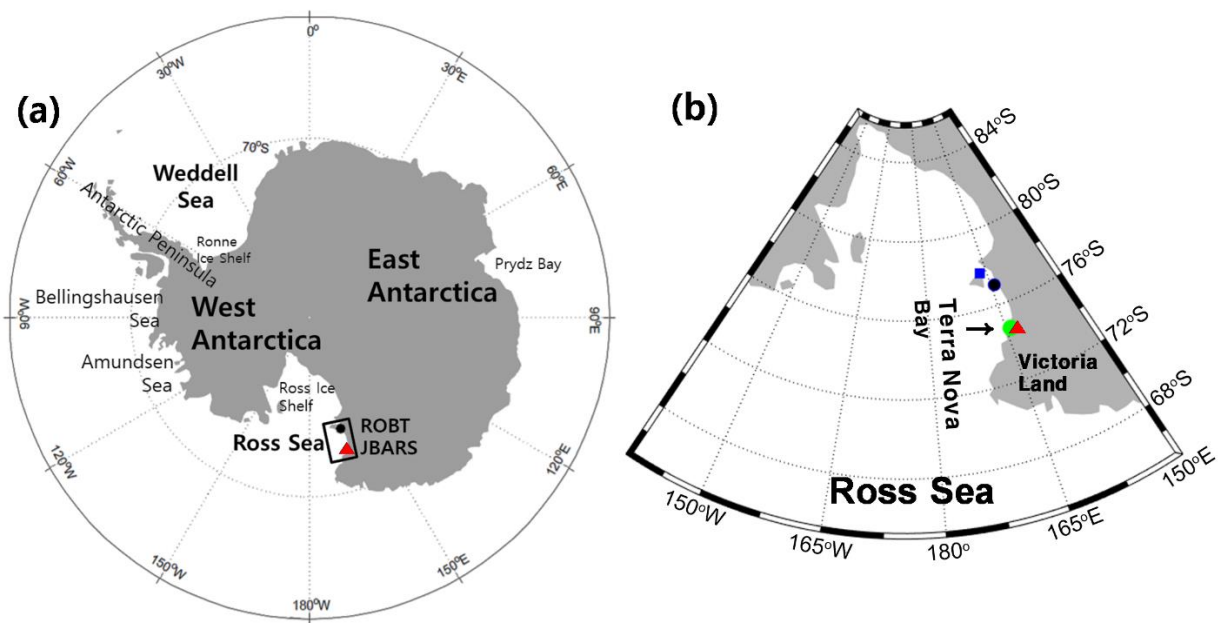
419 **Table 2. Harmonic constants for 6 long-period tidal constituents, derived from harmonic analysis of one year-long observations**
 420 **(2013) measured at the Cape Roberts sea level gauge (ROBT), using T_Tide (Pawlowicz et al., 2002). Note that this gauge is a vented**
 421 **piezometer so caution should be exercised in interpreting the results (particularly for S_a and S_{sa}) given the inclusion of**
 422 **proportionately large non-tidal (atmospheric) variations in this kind of sea level record**

Constituent		Amplitude (cm)	Amplitude standard error (cm)	Phase lag (°)	Phase lag standard error (°)	SNR
Solar annual	S_a	5.8	4.8	75	50	1.5
Solar semi-annual	S_{sa}	0.1	3.3	352	194	0.06
Lunar monthly	MS_m	0.4	3.5	57	254	0.02
	M_m	2.9	3.8	139	102	0.59
Lunar fortnightly	MS_f	1.2	3.0	281	189	0.14
	M_f	2.7	3.9	153	101	0.47

423 **Phase lags are referenced to 0° Greenwich, and SNR denotes the signal-to-noise ratios.**

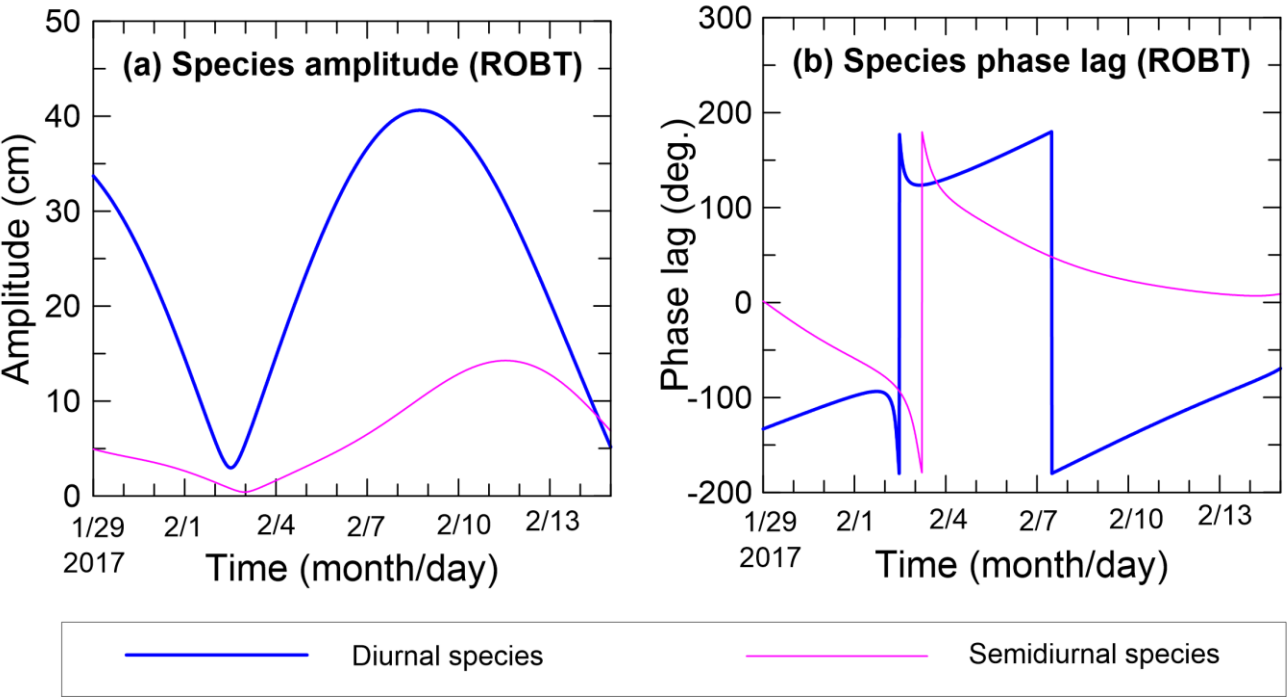


425
426 **Figure 1. Drifting ice, including icebergs and mobile sea ice, around the Jang Bogo Antarctic Research Station (JBARS),**
427 **photographed on 29 Jan. 2017.**



429

430 **Figure 2. Maps showing (a) the locations of the two tidal observation stations employed in this study within a wider Antarctic context:**
431 **Jang Bogo Antarctic Research Station (JBARS, ▲) and Cape Roberts (ROBT, ●); and (b) the case study station locations relative**
432 **to two other (previous) temporary tidal observations stations, McMurdo Station (■), and Mario Zucchelli Station (●), in the Ross**
433 **Sea.**



435

436 **Figure 3. Modulated tidal (a) species amplitudes and (b) phase lags for the diurnal and semidiurnal tidal species, calculated from**
437 **Cape Roberts (ROBT) tidal prediction data (29 Jan. to 14 Feb. 2017), using Appendix 1 Eqs. (A1) and (A3).**

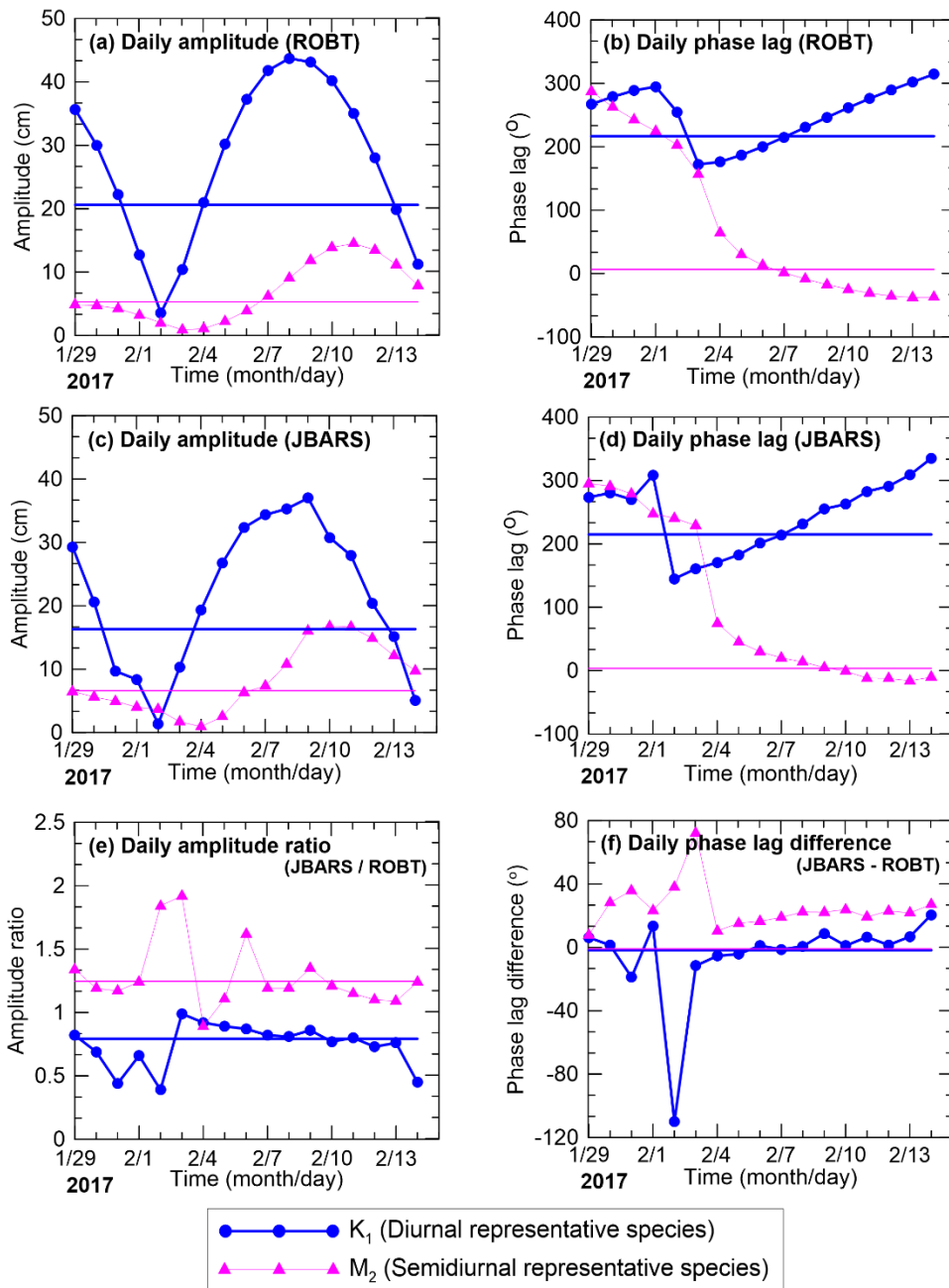


Figure 4. Daily amplitudes (a, c); phase lags (b, d); amplitude ratios (e); and phase lag differences (f) of the K_1 and M_2 tides (representative diurnal and semidiurnal tide species) at ROBT (a, b) and JBARS (c, d), and between JBARS and ROBT (e, f), calculated from ‘daily’ slices of the 29 Jan. to 14 Feb. 2017 ROBT tidal predictions and JBARS sea level observations. In addition, thick blue (K_1) and thin pink (M_2) horizontal lines in the panels indicate the amplitudes and phase lags derived from harmonic analyses of the entire 369 day 2013 ROBT sea level record (a, b) and of the entire 17 day 2017 JBARS sea level record (c, d), along with their amplitude ratios and phase lag differences (e, f).

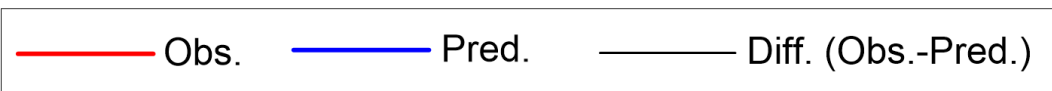
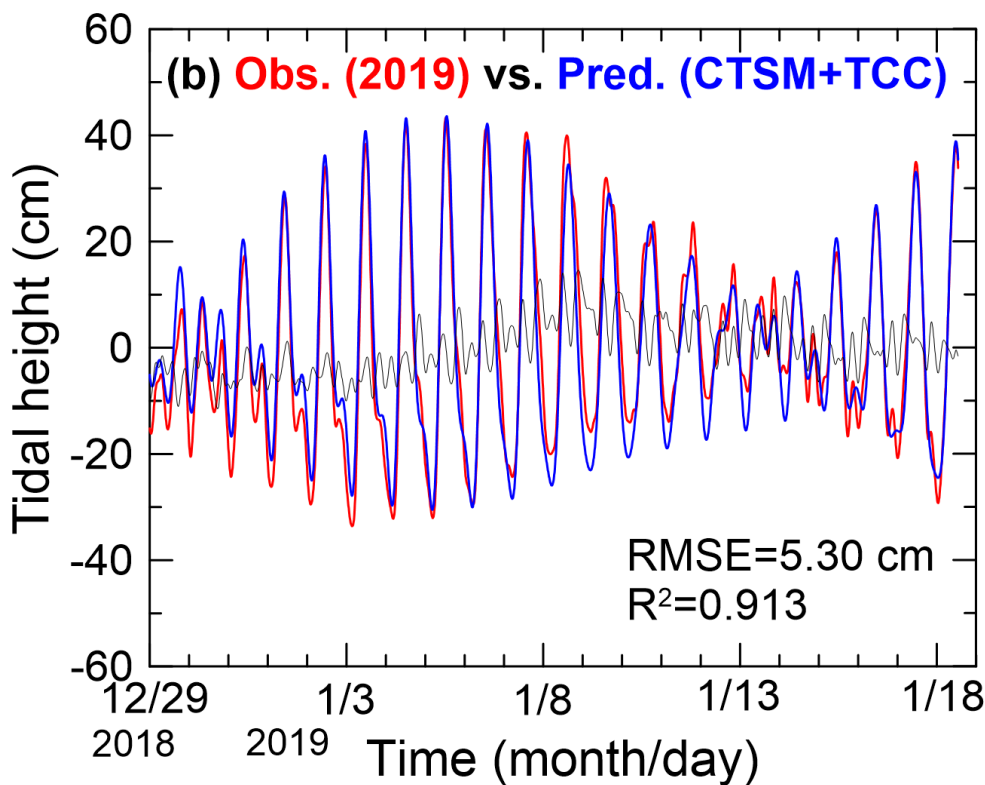
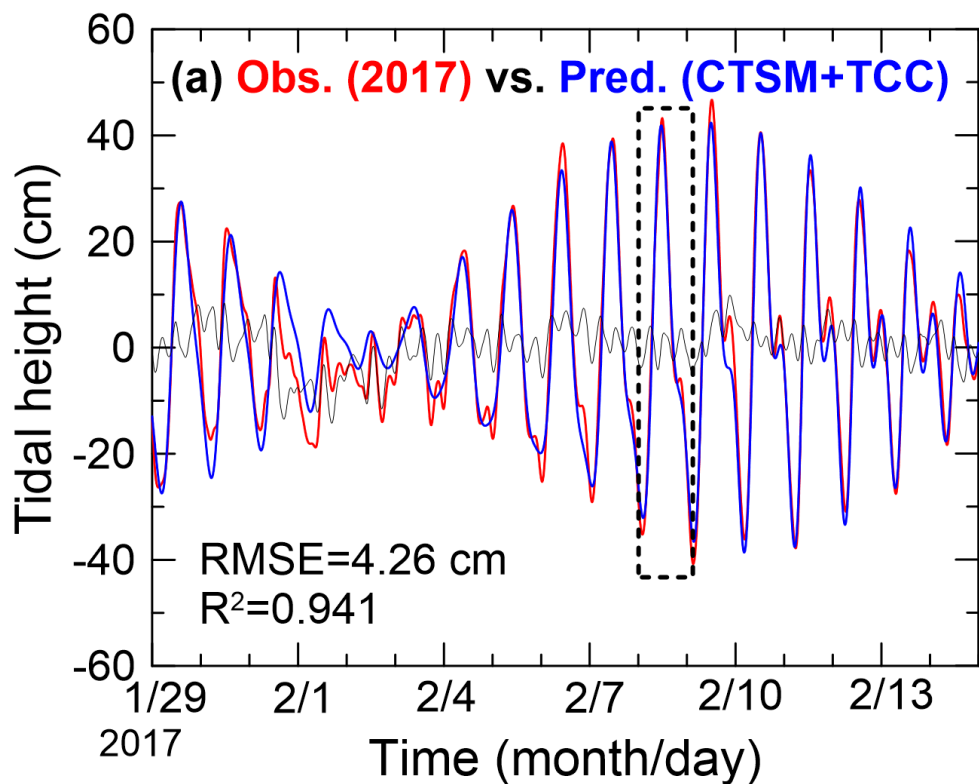


Figure 5. Time series of JBARS sea level observations (Obs.), predicted tidal heights (Pred.), and sea level residuals (Diff.) from (a) 29 Jan. to 14 Feb. 2017; and (b) 29 Dec. 2018 to 18 Jan. 2019. The JBARS predictions were generated via the CSTM+TCC method using a daily (25 hr) slice of local sea level observations from 8 Feb. 2017 (dashed box in (a)), along with concurrent (to time periods a and b) ROBT predictions; and year-long (2017) 5 min interval ROBT tidal predictions. RMSE and R² denote the comparison Root Mean Square Errors and coefficients of determination, respectively.

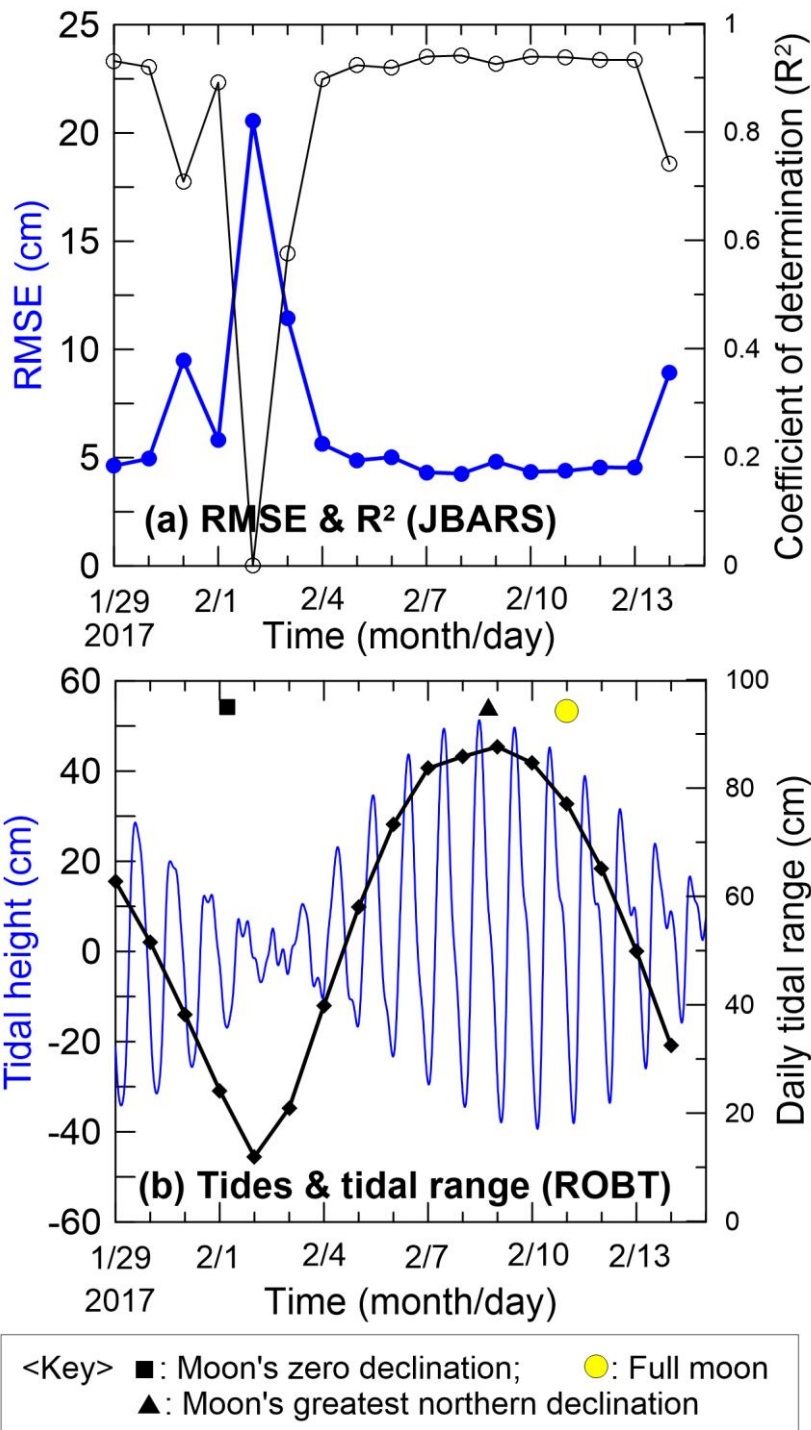
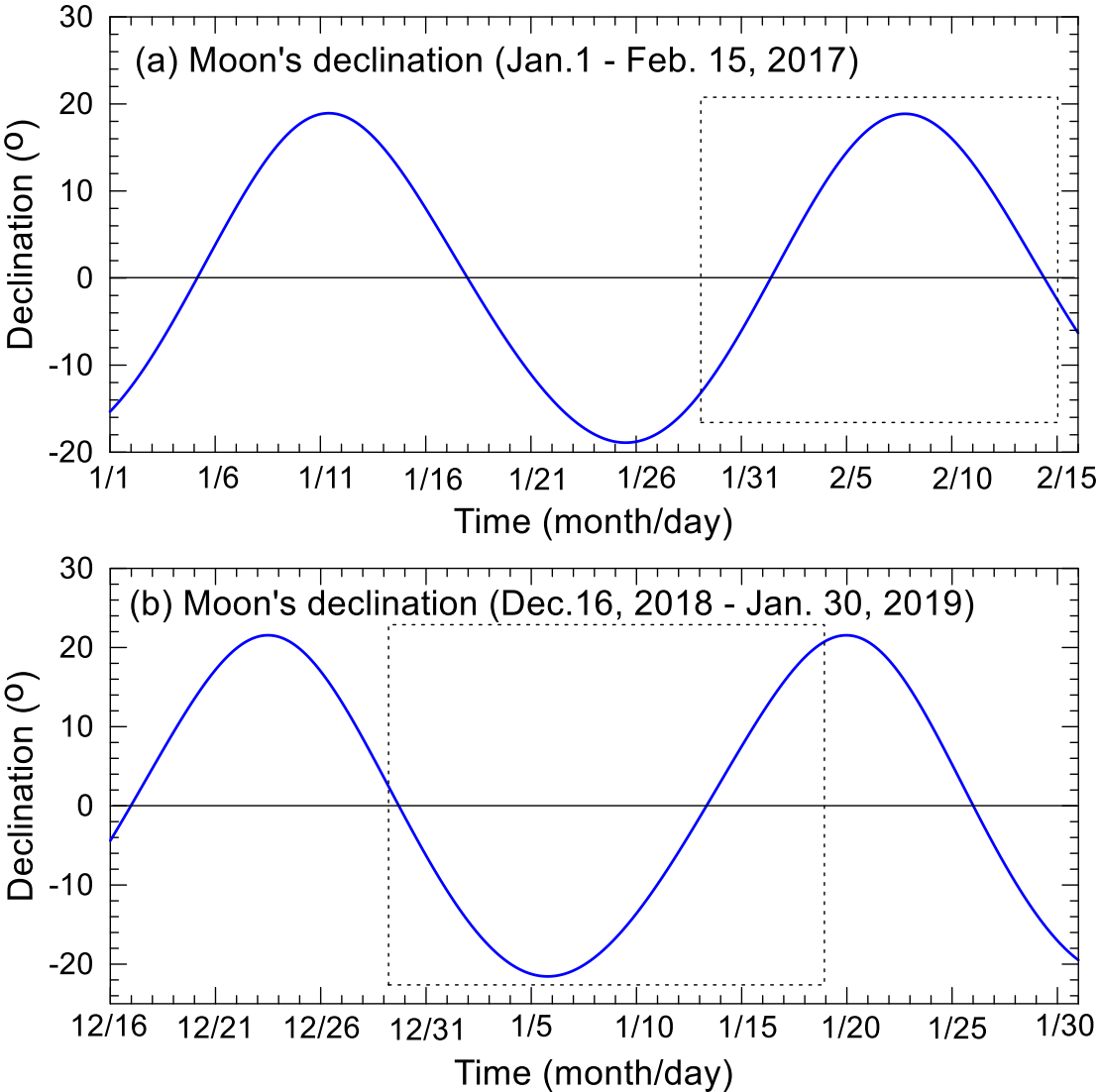


Figure 6. (a) Time series (29 Jan. to 14 Feb. 2017) of Root Mean Square Errors (RMSE, thick blue line with ●) and coefficients of determination (R², thin black line with ○) between JBARS 10 min interval sea level observations and the CTSM+TCC prediction datasets, generated for this site using harmonic analysis results from the JBARS daily (25 hr) sea level data slices and concurrent daily (25 hr) 2017 tidal prediction data slices and harmonic analysis results from ROBT station's year-long (2017) tidal predictions. (b) Time series of predicted 2017 tidal heights (thin blue line) and daily tidal ranges (thick black line with ♦) for ROBT, based on harmonic analysis of this station's 2013, 5 min interval sea level record, plus an indication of the moon's phase and declination.

462
463



464
465
466

Figure 7. Time series of the Moon’s declination, calculated at daily intervals for two observation periods: (a) 1 Jan. to 15 Feb. 2017; and (b) 16 Dec. 2018 to 30 Jan. 2019. Dashed boxes indicate the sea level observation windows examined in this study.

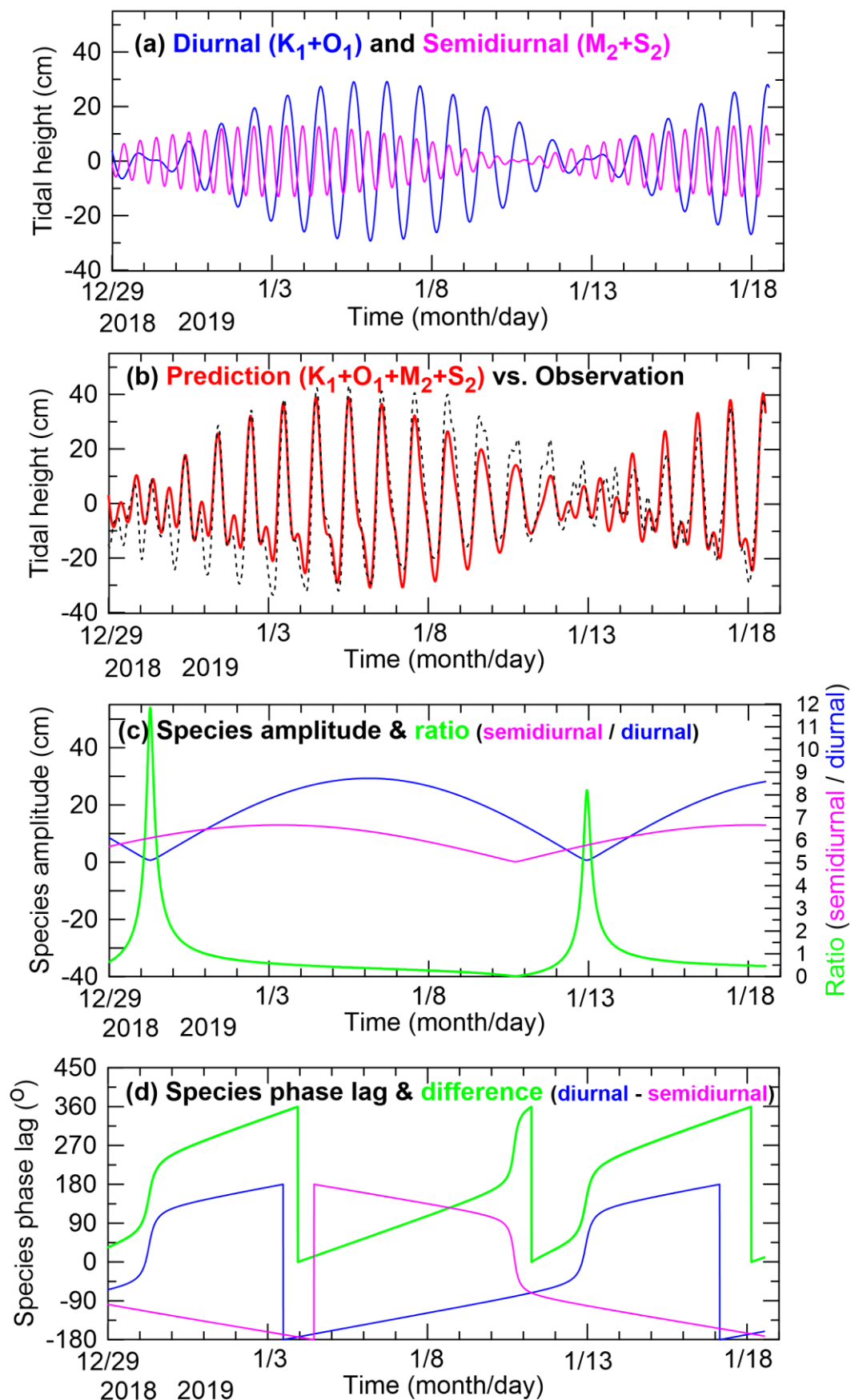
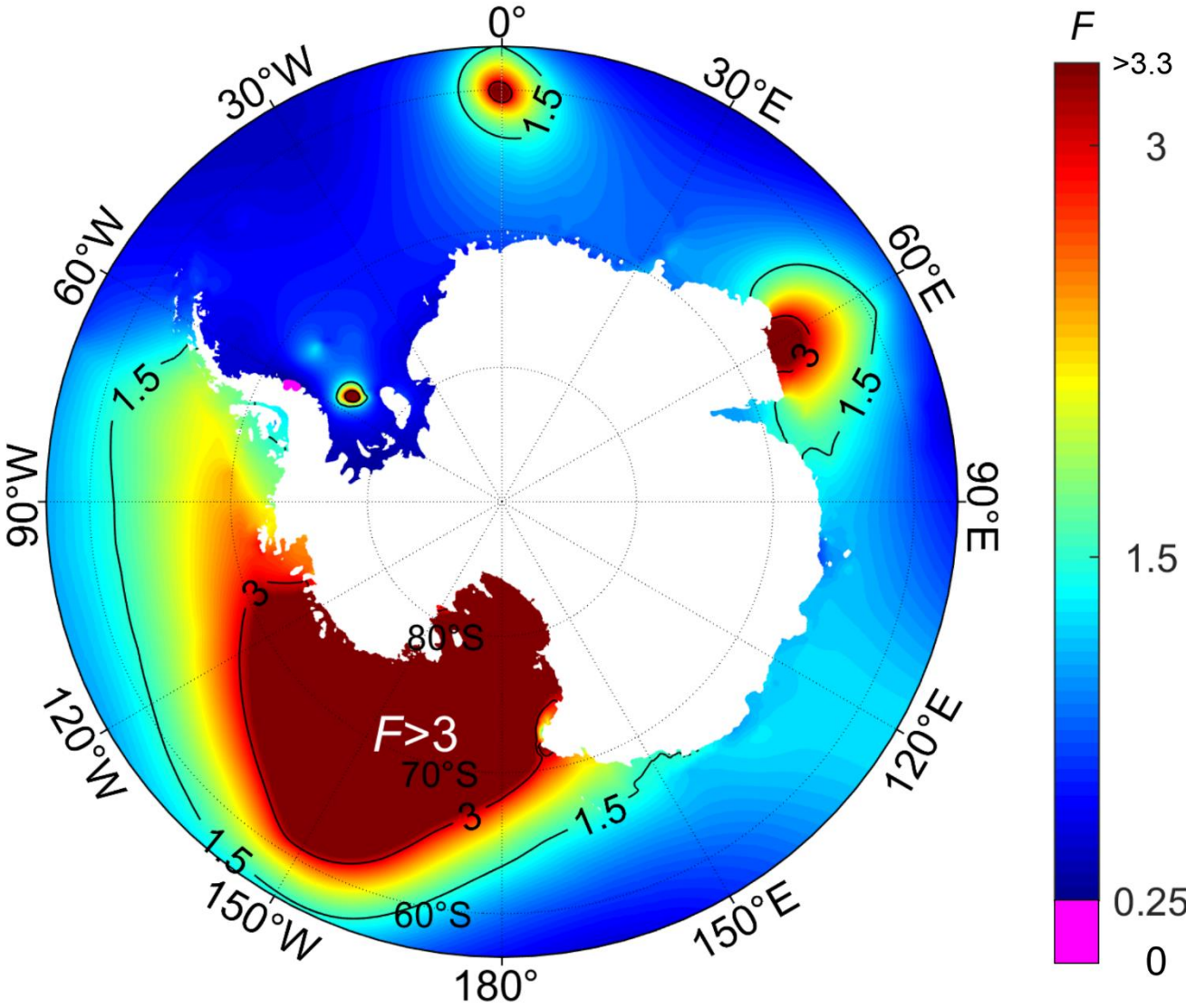


Figure 8. Time series (29 Dec. 2018 to 18 Jan. 2019) of (a) predictions of the diurnal (K_1+O_1) tides (blue line) and the semidiurnal (M_2+S_2) tides (magenta line) for JBARS; (b) their combined JBARS predictions (red line) and observations (black dashed line); (c) the ROBT diurnal (blue line) and semidiurnal (magenta line) species amplitudes and their ratio (green line); and (d) the ROBT diurnal (blue line) and semidiurnal (magenta line) species phase lags and their difference (diurnal – semidiurnal) (green line).



473

474 **Figure 9. Distribution of tidal form factor (F) values around Antarctica. Note the magenta area (72°S) on the Antarctic Peninsula's**
475 **Weddell Sea coast denotes the only area with a properly semidiurnal tide regime ($F < 0.25$) in the Antarctic region.**